AIMS *Biophysics*

Research article

Thermal investigation of montmorillonite/BSA by fourier transform infrared spectroscopy measurements[1]

Maria Teresa Caccamo[1],*, Giuseppe Mavilia[1], Letterio Mavilia[2], Pietro Calandra[3], Domenico Lombardo[4] and Salvatore Magazù[1]

[1] Dipartimento di Scienze Matematiche e Informatiche, Scienze Fisiche e Scienze della Terra, Università di Messina, Viale Ferdinando Stagno D'Alcontres n 31, S. Agata, 98166 Messina, Italy

[2] Dipartimento di Patrimonio, Architettura e Urbanistica; Università Mediterranea di Reggio Calabria, (PAU), Via Melissari, I‑89124 Reggio Calabria, Italy;

[3] Consiglio Nazionale delle Ricerche, Istituto per lo Studio Materiali Nanostrutturati, Via Salaria Km 29,300 00015 Monterotondo Stazione (Roma), Italy

[4] CNR–IPCF, Istituto per i Processi Chimico Fisici – (Sez. Messina) Viale F. Stagno D'Alcontres, 37. I-98158, Messina, Italy

* Correspondence: mcaccamo@unime.it; Tel: +390906765019.

Abstract: This paper reports the analysis of the intramolecular OH stretching band obtained by Fourier Transform Infrared (FTIR) spectroscopy measurements. In order to characterize the effect of montmorillonite on the properties of Bovine Serum Albumin (BSA) the two-state model is adopted for the analysis of the OH stretching band. We assume that the OH stretching can be divided into two different states of inter-molecular bonding. The results of this experimental work confirm that the montmorillonite leads to a stabilization of the BSA structure. Also, the analysis of the spectra temperature dependence shows a montmorillonite-induced higher thermal stability of the BSA in respect to pristine BSA. Thus, this paper highlights the effectiveness of montmorillonite as thermal bio-protector. A FTIR analysis was carried out to investigate the interaction of Montmorillonite with BSA. Two different approaches, i.e. Spectral Distance and Wavelet analyses, constitute two effective and innovative approaches for the characterization of the thermal properties of pristine BSA and of BSA in the presence of Montmorillonite. The results allowed us to consider as BSA in the presence

---

[1] "A previous version of this article contained parts of the Introduction reproduced from another published work, while all the Materials and Method, Results and Discussion and Conclusion sections were original.

The article has been, therefore, rectified by the authors upon solicitation of the Editors. The Editors would like to extend their sincere apologies for this fact and for any inconvenience it may have caused. The rectification notice appears as footnote in the new version of the original paper."

of Montmorillonite has a lower spectral sensitivity when the temperature changes and, therefore, the role of Montmorillonite as a thermal bio-protector is motivated.

1. Introduction

Many theories have been proposed on the origins of life on earth: in the Russian book of 1924, Oparin hypothesized that simple molecules (CH_4, NH_3) reacted to form small bio-molecules and bio-polymers (nucleotides, peptides,). They, then, evolve in multimolecular systems and, finally, they gave rise to the first forms of life [1]. Later, in a book of 1929, Haldane proposed a similar theory about the origins of life [2]: but, it was Bernal (1951) that suggested that clays had a fundamental role in chemical evolution and in the origins of life due to their ability to absorb, protect from ultraviolet radiation and catalyze the polymerization of organic molecules [3]. Then, Cains-Smith (1982) has proposed that clays can act as genetic candidates [4]. Hence, the inclusion of organic molecules and monomers in the layered structure of clays, such as montmorillonite and kaolinite, would favor the formation and replication of biopolymers such as enzymes and polynucleotides. Several literature works have shown that montmorillonite could be considered the cradle of the evolution of the early life forms on earth [5–19], also on the basis of its peculiar interaction with water [20–25]. From a general point of view, silicate-based clays [26–29] are classified in minerals of type 1: 1, such as kaolinite, and in minerals of type 2:1, such as montmorillonite which is characterized by weak bonds between interlayers [30–35] with excess negative charges [36–39].

The interlayer space of montmorillonite depends on the degree of hydration of the mineral: by increasing the number of water layers, the crystalline lattice expands (Figure 1); by complete dehydration, however, it loses its ability to expand. In fact, in the presence of water, H_2O molecules dispose themselves within the montmorillonite interlayer space, generating an increased space between the layers.
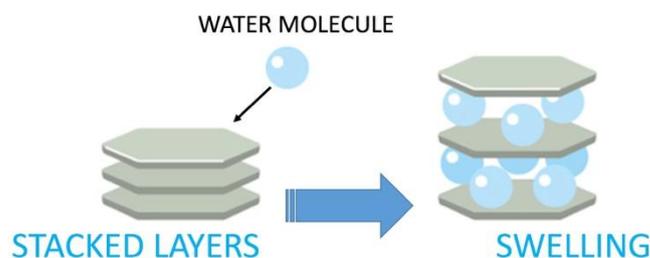

Figure 1. Swelling of montmorillonite clay in water.

Regarding the water absorption capacity, this property is very important for these clays. In fact, clays can absorb or desorb water as a function of changes in the moisture content: as above reported, when H_2O molecules are absorbed, they fill the space between the various layers. Montmorillonite has excellent water absorption properties; however, the interaction between the water molecules and

montmorillonite can produce swelling. The absorption of water molecules and the swelling of montmorillonite determine to the formation of hydrated states and can give rose to hysteresis phenomena. The montmorillonite swelling and hydration processes play a fundamental role for a wide variety of engineering applications. Furthermore, the anisotropy of a wide class of clays is reflected in a broad variable range of mechanical properties. The structure of hydrated montmorillonite is shown in Figure 2: this anisotropy of montmorillonite can produce great differences in the values of elastic constants, shear modulus, and Young's modulus. Moreover, these mechanical properties decrease with increasing hydration [40–42]. Furthermore, as regards the thermal properties, montmorillonite is a good thermal insulator and, moreover, it allows to increase the thermal stability once added as an additive in many materials. Recent developments in the use of self-assembling supramolecular objects to fabricate innovative well-defined nanomaterials links soft matter chemistry to hard matter sciences [43–46] and requires the employment of techniques and approaches that to simultaneously detect the structure re-organization and dynamics at the nanoscale [47–49]. This is a significant area of research to produce thermal barrier effects in the structure of the composite material: in fact, the thermal barrier properties of clays are appreciated in many applications involving the use of heat-resistant materials and flame retardants. The nanoclays have been largely studied and used in polymer matrix composites to obtain greater thermal stability and better flame retardancy properties. The variation of thermal expansion, under the effect of heat, for metals, polymers and ceramics was analyzed: generally, the order of magnitude of the thermal expansion in polymers, metals and ceramics can be indicated as follows: polymer > metal > ceramics. This order is based on the values of the linear thermal expansion coefficient in the values range 20–100, 3–20 and 3–5 ppm/℃ for polymers, metals and ceramics, respectively [50]. Therefore, a higher thermal stability of montmorillonite allows its use as a filler in polymers to make composite materials with a low coefficient of thermal expansion. However, the improvement of the thermal stability of the polymers requires an increase in the ratio between surface and volume of a material (aspect ratio) and, therefore, can be obtained for values of this aspect ratio higher than 100. Several investigations have been addressed to clarify the role played by ribonucleic acid (RNA) in the early life forms [12,51–64] and on the montmorillonite bioprotective effects on RNA oligomers [12,65–67].

The development of advanced nanomaterials exploit the self-assembly process that involves the combination of non-covalent soft interactions with the multi-functionality of building blocks and provides an excellent strategy for the preparation of novel, advanced nanomaterials with highly controlled properties for biotechnology and material science application [68–71]. Previously, it has been highlighted that clays have a high specific surface, cation exchange capacity and absorption capacity and, therefore, they are appreciated for their high absorption capacity of cations including Ag^+, Zn^{2+} and Cu^{2+}. Furthermore, previous research in the literature has shown that clays modified with these cations have antibacterial properties [72–77]. As regards, however, the antibacterial properties of montmorillonite modified with Fe^{3+} cations, some studies in the literature have shown effective removal of phenolic organic compounds from wastewater due to the oxidative oligomerization catalyzed on the surface by the same Fe^{3+} saturated montmorillonite [78–80]. Moreover, it has been hypothesized that the Fe^{3+} saturated montmorillonite could also be able to eliminate the bacteria present in the wastewater. Although montmorillonites modified with Cu^{2+}, Zn^{2+} and Ag^+ cations show antibacterial activity, the presence of these cations in water could pose a potential risk to public health due to their toxicity at high concentrations. Therefore, it was proposed to use the saturated montmorillonite of Fe^{3+} as a possible alternative for the water disinfection process because iron is an essential element for humans [81]. In

summary, the effectiveness of Fe^{3+} saturated montmorillonite for the elimination of bacteria present in secondary wastewater has been demonstrated. So, these experimental results suggest as the montmorillonite modified with Fe^{3+} cations could probably be used as an effective antibacterial material for water disinfection in small plants used for the treatment of drinking water and in large plants used for the treatment of drinking water and wastewater. In this experimental work, samples of Montmorillonite and its mixture with Bovine Serum Albumin (BSA) were investigated as a function of temperature by means of Fourier Transform Infrared (FTIR) spectroscopy technique and Spectral Distance (SD) approach. In order to determine the thermal protective effects of Montmorillonite on a system of biophysical interest, a protein, the Bovine Serum Albumin (BSA) was chosen [82–89]. It is a serum albumin protein derived from cows and it has numerous biochemical applications such as ELISAs (Enzyme-Linked Immunosorbent Assay) and immunohistochemistry [90–95]. Bovine Serum Albumin (BSA) is a small, soft, stable, non-reactive protein, and it is used as a representative short peptide in the drug delivery system [96–101]. It is well known that exist different techniques to investigate the behaviours of proteins, such as X-rays, Nuclear Resonance Magnetic, Neutron Scattering, Dynamic Light Scattering, Acoustic Levitation, Raman spectroscopy and InfraRed absorption [102–110].

2.   Materials and method

Pristine montmorillonite powders purchased from Merck (Milano, Italy, surface area 250 m^2/g), BSA (purchased from Sigma) and double distilled water were used to prepare the samples. Montmorillonite/water mixtures have been prepared by adding to pure protein double-distilled water (80 wt% Montmorillonite); for Montmorillonite/water/BSA mixtures the concentration was: 80 wt% Montmorillonite/20 wt% (BSA (50 wt%) + H_2O (50 wt%)). Fourier Transform InfraRed (FTIR) spectroscopy allows us to characterize the molecule rotational and vibrational motions. This spectroscopic technique explores 14000–10 cm^{-1} range of the electromagnetic spectrum, which encloses the Near-IR range (14000 ÷ 4000 cm^{-1}), the Mid-IR range (4000 ÷ 400 cm^{-1}), and the Far-IR (400 ÷ 10 cm^{-1}). FTIR technique is a powerful method to investigate the structural and dynamical properties of materials as well as their dependence on temperature: this technique is based on the analysis of the absorption spectra [111–114]. In this experimental work, we collected vibrational spectra by means of the Vertex 70 v spectrometer (Bruker Optics, Ettlingen, Germany) using a Platinum diamond ATR. All spectra were collected by using an average of 96 scans with a resolution of 4 cm^{-1} in a spectral range of 4000–400 cm^{-1}, from a temperature of 20 ℃ to 55 ℃. The pre-processing data procedure was performed through OPUS software and, then, by means of Matlab environment. Due to the complexity of the investigated systems we prefer to analyze globally the spectral features of the samples by applying an innovative approach consisting in the integrated use of the Spectral Distance and Wavelet Cross Correlation protocols. Such an approach reveals to be very effective since in the present study we focus the attention only on the spectra temperature dependence. On this purpose, to characterize the temperature sensitivity of the analyzed samples, the Spectral Distance approach has been used; this latter is based on the following expression:

$$SD = \left(\sum [A(\omega, T) - I(\omega, T_l)]^2 \cdot \Delta\omega \right)^{\frac{1}{2}} \tag{1}$$

where $A(\omega)$ represents the absorbance at the frequency ω, T_l denotes the lowest temperature, that is 20 ℃ and $\Delta\omega$ is the frequency resolution of the instrument.

3. Results and discussion

In Figure 2, the FTIR spectrum of Montmorillonite in the spectral range of $4000 \div 400$ cm^{-1} at the temperature of T = 20 ℃ is reported.

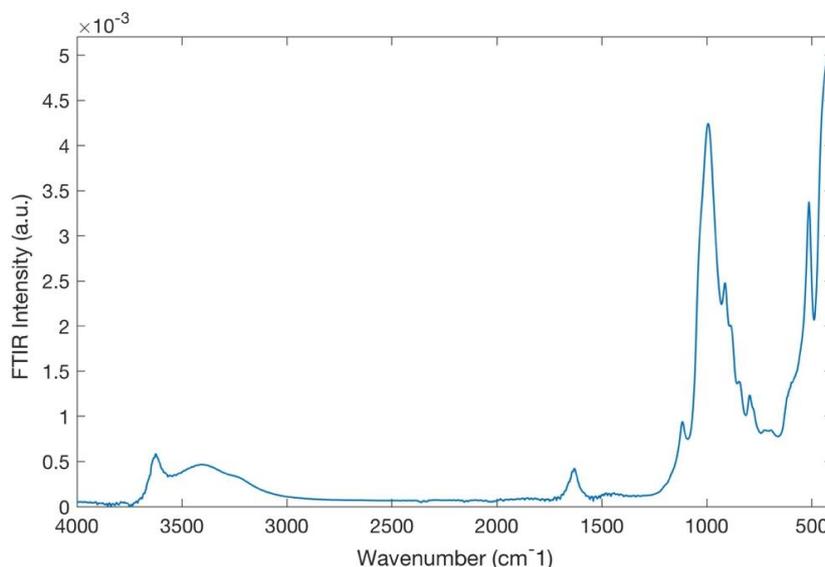**Figure 2.** FTIR spectrum of Montmorillonite in the resolution spectral range of 4000 $\div$ 400 cm^{-1} at the temperature of T = 20 ℃.
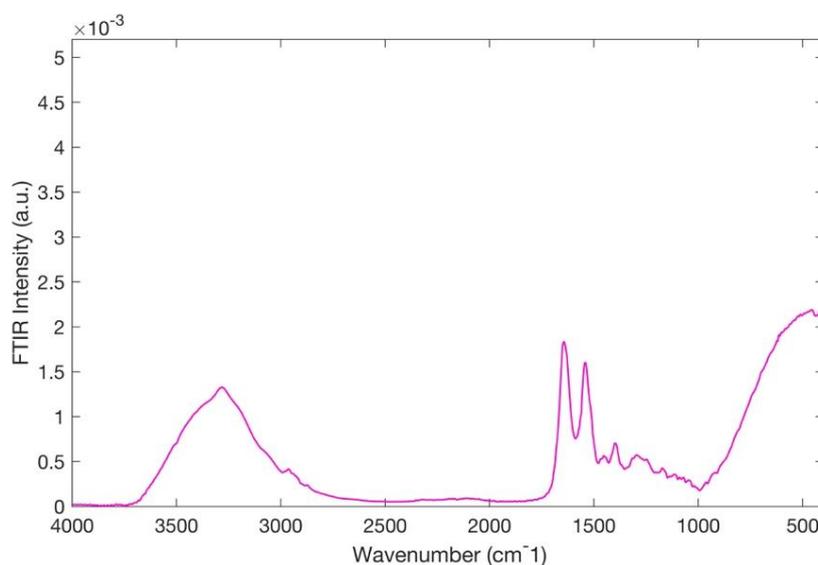

Figure 3. FTIR spectra of the BSA in the resolution spectral range of 4000 $\div$ 400 cm^{-1} at temperature T = 20 ℃.

The most significant peaks are located at ~ 3632 cm^{-1}, i.e. O-H stretching; at ~ 1639 cm^{-1} that represents the O-H bending (hydration) ; at ~ 1113 cm^{-1} and 1035 cm^{-1} make reference to the i-O stretching, out of plane and in plane, respectively. Finally, the peak at ~915 cm^{-1} denotes the AlAlOH bending, at ~793 cm^{-1} is situated the tridymite peak and the peak at ~529 cm^{-1} represents the Si-O

bending vibration. Figure 3 shows the FTIR spectrum of BSA in the spectral range of $4000 \div 400$ cm^{-1} at at the temperature of T = 20 ℃.

For the FTIR BSA spectrum, one of the most important IR spectral feature for the protein are the bands of Amide. In particular, in Figure 3, there are at ~ 3292 cm^{-1} the Amide A, at ~ 1649 cm^{-1} Amide I and at ~ 1537cm^{-1} Amide II. Figure 4 reports the FTIR spectra for Montmorillonite/water mixtures in the spectral range of $4000 \div 400$ cm^{-1} and in the temperature range of 20 ℃ $\div$ 55 ℃.
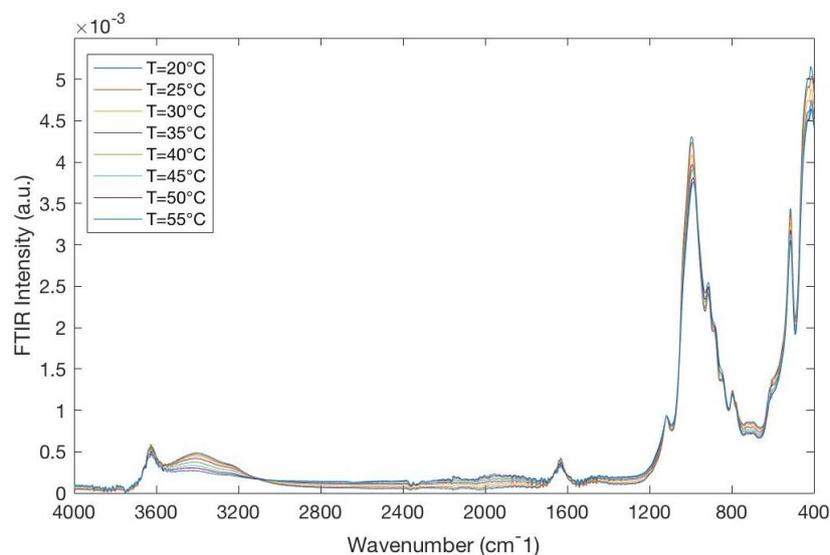

Figure 4. FTIR spectra for Montmorillonite/water mixtures in the spectral range of $4000 \div 400$ cm^{-1} and in the temperature range of 20 ℃ $\div$ 55 ℃.

Figure 5. FTIR spectra for Montmorillonite/water mixtures/BSA in the spectral range of $4000 \div 400$ cm^{-1} and in the temperature range of 20 ℃ $\div$ 55 ℃.

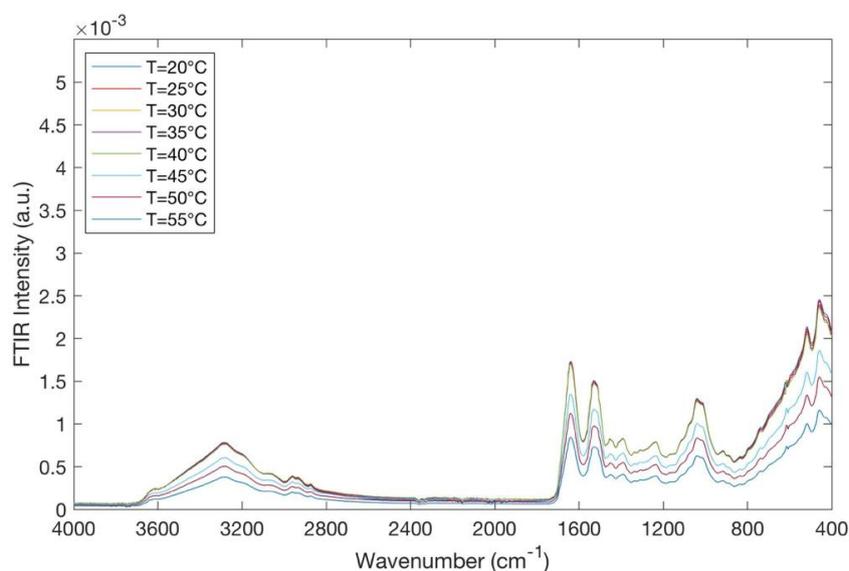Figure 5 shows the FTIR spectra for Montmorillonite/water mixtures/BSA in the spectral range of $4000 \div 400$ cm^{-1} and in the temperature range of 20 ℃ $\div$ 55 ℃.

As it can be seen, in Figure 5, the typical IR bands of Montmorillonite and the peaks of Bovine Serum Albumin (BSA) are observed. More precisely, by increasing temperature a little decrease in IR band intensity at ~3440 cm^{-1} of the O-H stretching band is observed; this suggests a dehydration of Montmorillonite. The peaks at ~1649 and at 1537 cm^{-1} are typical of BSA and can be attributed to the C=O stretching vibration of the peptide linkages; they turn out to be very sensitive to the secondary structural components of the protein. These two peaks decrease with increasing temperature.
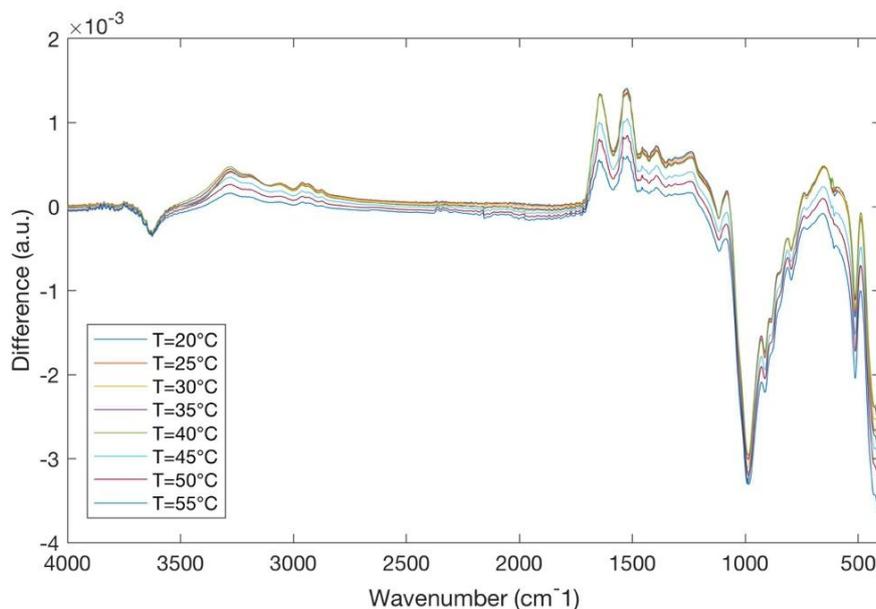

Figure 6. Spectra differences in the temperature range 20 ℃ $\div 55$ ℃.

Before to proceed with the analysis of data, a pre-processing data procedure was performed by eliminating the background. To better investigate the mechanisms of interactions that occur between Montmorillonite and BSA, the spectrum difference has been taken into account. In particular, from the spectrum of Montmorillonite in the presence of BSA, the spectrum of Montmorillonite has been subtracted the spectrum of Montmorillonite so obtaining the spectrum difference. This procedure was adopted for each spectra of all the investigated temperatures. In Figure 6, the spectra differences, in the temperature range 20 ℃ $\div 55$ ℃, are reported.

The thermal behaviour of the investigated systems was characterized by the evaluation of SD (eq. 1). Figure 7 reports SD as a function of temperature for BSA (green circle) and for the spectrum difference (light blue square) together with their linear fits.
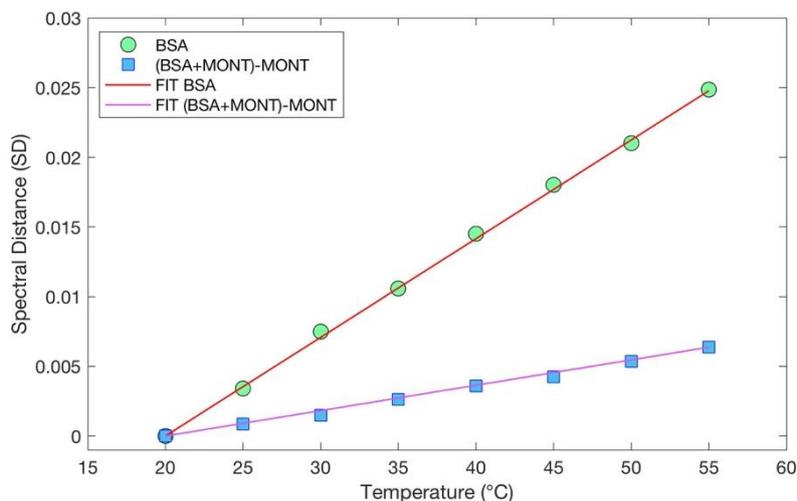
Figure 7. SD as a function of temperature for BSA (green circle) and for BSA in the presence of Montmorillonite (light blue square) together with their linear fits (continuous lines).

In order to extract quantitative information, a linear fit has been performed:

$$Y = ax + b \qquad (2)$$

By this examination, it results that the slope coefficient value for the spectrum difference, $m = 1.82 \cdot 10^{-4}$, is lower than the slope coefficient value for BSA, that is equal to $m = 7.08 \cdot 10^{-4}$. This suggests that BSA in presence of Montmorillonite has a higher thermal resistance and for this reason Montmorillonite can be considered as an effective thermal bioprotector.

Another approach to investigate the thermal behavior of Montmorillonite consists in applying the wavelet cross correlation method, that allows to determine, evaluating the wavelet cross-correlation coefficient, r_{XWT}, the degree of affinity between two signals. Such a method is very innovative and powerful and is employed in several kinds of disciplines such as climate, geoscience, physics, mathematics, finance, engineering science and others [115–120]. Let's consider two wavelet transforms, $W_1(s,\tau)$ and $W_2(s,\tau)$ of the investigated spectra, where s represents the scale parameter ($s > 0$) and τ denotes the shift parameter, and the two wavelet spectra $P_1(s)$ and $P_2(s)$ [121–125]. From a mathematical point of view $W(s,\tau)$ is the inner product of the function $f(x)$ and scaled and shifted mother wavelets ψ:

$$w(a,\tau) = \frac{1}{a} \int_{-\infty}^{+\infty} f(x)\psi^*|x-\tau|\,dx;$$

where $f(x)$ denotes the one-dimensional function, * is the complex conjugate, and ψ is the mother wavelet:

$$\psi_{s,\tau} = \frac{\psi(x-\tau)}{s}; \qquad (3)$$

then, one defines the wavelet spectrum $P(s)$:

$$P(s) = \frac{1}{s} |w(s, \tau)|^2 dx;$$ (4)

and finally, one determines the wavelet cross-correlation coefficient, r_{XWT}:

$$r_{XWT}(s) = \frac{\int W_1(s, \tau) W_2^*(s, \tau) d\tau}{\sqrt{P_1(s) P_2(s)}}$$ (5)

The wavelet cross-correlation coefficient varies in the range $-1 \leq r_{XWT} \leq 1$; if the value is equal to 1 indicates a positive statistical relationship between the spectra; if the value is equal to 0 no statistical relationship between spectra exists; finally, if the value is equal to −1 a negative correlation between the two spectra is present. In the present study, the spectrum at lowest temperature (T = 20 ℃) has been chosen as reference wavelet spectrum both for BSA and for the spectrum difference.
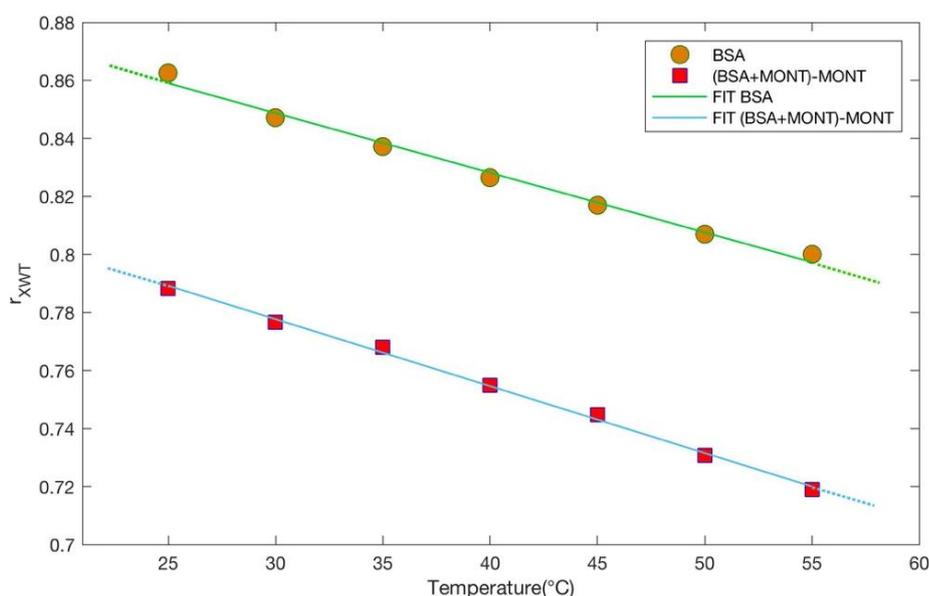

Figure 8. Wavelet cross-correlation coefficient, r_{XWT}, versus temperature together with their linear fits.

Figure 8 shows the evaluated wavelet cross-correlation coefficient, r_{XWT}, versus temperature for BSA (orange circles) and for the spectrum difference (magenta squares) together with their linear fits.

What it emerges is that r_{XWT} decreases by increasing temperature following a decreasing linear trend. Also in this case, a linear fit has been performed and the slope coefficient value for the spectrum difference, $m = 0.8159$ is lower than the slope coefficient value for BSA, that is equal to $m = 0.9245$. These results confirm that Montmorillonite can be considered as a thermal bioprotector.

4. Conclusion

The present experimental work has allowed to show the importance of Montmorillonite clay as a thermal bioprotector. FTIR data were collected to study the interaction of Montmorillonite with BSA. SD and wavelet analyses, constitute two effective and innovative approaches for the characterization of the thermal properties of pure BSA and of BSA in the presence of Montmorillonite. Both approaches suggest that BSA in the presence of Montmorillonite has a lower spectral sensitivity when the temperature changes and, hence, the role of Montmorillonite as a thermal bioprotector is thus justified.

Conflict of interest

The authors declare that there is no conflict of interest regarding the publication of this article.

References

1. Leach S (2015) Origins of life. *Adv Chem Phys* 157: 293–313.
2. Haldane JBS (1929) The origin of life. *Rationalist Annual* 148: 3–10.
3. Bernal JD (1949) The physical basis of life. *P Phys Soc* 62: 597.
4. Cains-Smith AG (1982) *Genetic Takeover*. Cambridge: Cambridge University Press.
5. Lehn JM (2002) Toward complex matter: Supramolecular chemistry and self-organization. *PNAS* 99: 4763–4768.
6. Lehn JM (2002) Toward self-organization and complex matter. *Science* 295: 2400–2403.
7. Bada JL, Lazcano A (2003) Perceptions of science. Prebiotic soup-revisiting the Miller experiment. *Science* 300: 745–746.
8. Watson JD, Crick FHC (1953) Molecular structure of nucleic acids. *Nature* 171: 737–738.
9. Troland LT (1914) The chemical origin and regulation of life. *The Monist* 22: 92–133.
10. Muller HJ (1961) Genetic nucleic acid: Key material in the origin of life. *Persp Biol Med* 5: 1–23.
11. Gilbert W (1986) Origin of life: The RNA world. *Nature* 319: 618–618.
12. Chaabani H (2015) Man creation had began since the creation of the first biological material very likely in Clay. *Int J Mod Anthrop* 8: 49–65.
13. Luisi PL (2006) *The Emergence of Life. From Chemical Origins to Synthetic Biology.* Cambridge: Cambridge University Press.
14. Szostak JW, Bartel DP, Luisi PL (2001) Synthesizing life. *Nature* 409: 387–390.

15. Nielsen PE, Egholm M, Berg RH, et al. (1991) Sequence-selective recognition of DNA by strand displacement with a thymine-substituted polyamide. *Science* 254: 1497–1500.

16. Lazcano A (2010) Historical development of origins research. *Cold Spring Harbor Persp BioL* 2: a002089.

17. Wachtershauser G (1988) Before enzymes and templates, a theory of surface metabolism. *Microbiol Rev* 52: 452–484.

18. Haldane JBS (1954) The origins of life. *New Biol* 16: 12–27.

19. Muller HJ (1966) The gene material as the initiator and the organizing basis of life. *Am Naturalist* 100: 493–517.

20. Raven PH, Johnson GB, Mason KA, et al. (2014) The nature of molecules and properties of water. *Biology*, 10 Eds., New York: McGraw-Hill, 17–30.

21. Reece JB, Urry LA, Cain ML, et al. (2011). Water and life. *Campbell Biology,* 10 Eds., San Francisco: Pearson, 44–54.

22. Caetano-Anollés G, Wang M, Caetano-Anollés D (2013) Structural phylogenomics retrodicts the origin of the genetic code and uncovers the evolutionary impact of protein flexibility. *PLoS One* 8: e72225.

23. Eigen M, Lindemann BF, Tietze M, et al. (1989) How old is the genetic code? Statistical geometry of tRNA provides an answer. *Science* 244: 673–679.

24. Ertem G, Ferris JP (2000) Sequence and regio-selectivity in the montmorillonite catalyzed synthesis of RNA. *Orig Life Evo Biosph* 30: 411–422.

25. Farias ST, do Rego TG, José MV (2014). Evolution of transfer RNA and the origin of the translation system. *Fron Genet* 5 : 303–306.

26. Ghadiri M, Chrzanowski W, Rohanizadeh R (2015). Biomedical applications of cationic clay minerals. *RSC Adv* 5: 29467–29481.

27. de Paiva LB, Morales AR, Díaz FRV (2008) Organoclays: properties, preparation and applications. *App Clay Sci* 42: 8–24.

28. Datta M (2013) Clay–polymer nanocomposites as a novel drug carrier: Synthesis, characterization and controlled release study of Propranolol Hydrochloride. *Appl Clay Sci* 80–81: 85–92.

29. Xiang Y, Villemure G (1996) Electrodes modified with synthetic clay minerals: electrochemistry of cobalt smectites. *Clays Clay Miner* 44: 515–521.

30. Patel HA, Somani RS, Bajaj HC, et al. (2006) Nanoclays for polymer nanocomposites, paints, inks, greases and cosmetics formulations, drug delivery vehicle and waste water treatment. *Bull Mater Sci* 29: 133–145.

31. Yu WH, Li N, Tong DS, et al. (2013) Adsorption of proteins and nucleic acids on clay minerals and their interactions: A review. *Appl Clay Sci* 80–81: 443–452.

32. Stănescu VN, Olteanu M, Florea-Spiroiu M, et al. (2008) Fractal properties of collagen/chitosan/montmorillonite membranes. *Rev Roum Chim* 54: 767–771.

33. Raussell-Colom JA (1987) Reactions of clays with organic substances. *Chem Clays Clay Miner, Mineral Soc* 412–415.

34. Bergaya F, Lagaly G (2001) Surface modifications of clay minerals. *Appl Clay Sci* 19: 1–3.

35. Caccamo MT, Mavilia G, Mavilia L, et al. (2020) Self-assembly processes in hydrated montmorillonite by FTIR investigations. *Materials* 13: 1100.

36. Maina E, Wanyika H, Gachanja A (2016). Natural pyrethrum extracts photo-stabilized with organo clays. *J Sci Res Rep* 9: 1–20.

37. Ismadji S, Soetaredjo F, Ayucitra A, et al. (2015) Natural clay minerals as environmental cleaning agents. *J Clay Mat Environ Rem* 8: 5–37.

38. Celis R, HermosÍN C, Cornejo L, et al. (2010) Clay–herbicide complexes to retard picrolam leaching in soil. *Int J Environ Analyt Chem* 82: 503–517.

39. Xi Y, Frost RL, He H (2007) Modification of the surfaces of Wyoming montmorillonite by the cationic surfactants alkyl trimethyl, dialkyl dimethyl and trialkylmethyl ammonium bromide. *J Coll Interf Sci* 305: 150–158.

40. Savelyev YV, Gonchar AN (2019) Exfoliation of montmorillonite in polymer matrix and its influence on the nanocomposites properties. *Polym J* 41: 149–158.

41. Emiel JM, Hensen SB (2002) Why clay swell. *J Phys Chem B* 106: 12664–12667.

42. Tyagi B, Chudasama CD, Jasra RV (2006) Determination of structural modification in acid activated montmorillonite clay by FT-IR spectroscopy. *Spectrochim Acta A* 64: 273–278.

43. Temuujin J, Jadambaa T, Burmaa G, et al. (2004) Characterisation of acid activated montmorillonite clay from tuulant (Mongolia). *Ceram Int* 30: 251–255.

44. Bonaccorsi L, Calandra P, Kiselev MA, et al. (2013) Self-assembly in poly(dimethylsiloxane)-poly(ethylene oxide) block copolymer template directed synthesis of linde type A zeolite. *Langmuir* 29: 7079–7086.

45. Bonaccorsi L, Calandra P, Amenitsch H, et al. (2013) Growth of fractal aggregates during template directed SAPO-34 zeolite formation. *Microporous Mesoporous Mat* 167: 3–9.

46. Bonaccorsi L, Lombardo D, Longo A, et al. (2009) Dendrimer template directed self-assembly during zeolite formation. *Macromol* 42: 1239–1243.

47. Chen C, Wylie RAL, Klinger D, et al. (2017) Shape control of soft nanoparticles and their assemblies. *Chem Mater* 29: 1918–1945.

48. Kiselev MA, Lombardo D (2017) Structural characterization in mixed lipid membrane systems by neutron and X-ray scattering. *Biochem Biophys Acta-Gen Sub* 1861: 3700–3717.

49. Lombardo D, Munaò G, Calandra P, et al. (2019) Evidence of pre-micellar aggregates in aqueous solution of amphiphilic PDMS–PEO block copolymer. *PCCP* 21: 11983–11991.

50. Rao Y, Blanton TN (2008) Polymer nanocomposites with a low thermal expansion coefficient. *Macromolecules* 41: 935–941.

51. Huang W, Ferris JP (2006) One-step, regioselective synthesis of up to 50-mers of RNA oligomers by montmorillonite catalysis. *J Am Chem Soc* 128: 8914–8919.

52. He H, Guo J, Xie X, et al. (2002) Microstructural study of acid-activated montmorillonite from Choushan, China. *Clay Miner* 37: 337–344.

53. Ferris JP (2005) Mineral calalysis and prebiotic synthesis: Montmorillonite-catalyzed formation of RNA. *Elements* 1: 145–149.

54. Joshi PC, Pitsch S, Ferris JP (2000) Homochiral selection in the montmorillonite-catalyzed and uncatalyzed prebiotic synthesis of RNA. *Chem Comm:* 2497–2498.

55. Mazo MA, Manevitch LI, Gusarova EB, et al. (2008) Molecular dynamics simulation of thermomechanical properties of montmorillonite crystal. 3. Montmorillonite crystals with PEO oligomer intercalates. *J Phys Chem B* 112: 3597–3604.

56. Adams JM (1987) Synthetic organic chemistry using pillared, cation-exchanged and acid- treated montmorillonite catalysts—A review. *Appl Clay Sci* 1987: 309–342.

57. Miyakawa S, Ferris JP (2003) Sequence-and regioselectivity in the montmorillonite-catalyzed synthesis of RNA. *J Am Chem Soc* 125: 8202–8208.

58. Kawamura K, Ferris JP (1999) Clay catalysis of oligonucleotide formation: kinetics of the reaction of the 5'-phosphorimidazolides of nucleotides with the non-basic heterocycles uracil and hypoxanthine. *Orig Life Evol Biosph* 29: 563–591.

59. Joshi PC, Aldersley MF, Delano JW, et al. (2009) Mechanism of montmorillonite catalysis in the formation of RNA oligomers. *J Am Chem Soc* 131: 13369–13374.

60. Knauth LP (1998) Salinity history of the earth's early ocean. *Nature* 395: 554–555.

61. Knauth LP (2005) Temperature and salinity history of the precambrian ocean: Implications for the course of microbial evolution. *Palaegeogr Palaeoclimatol Palacoecol* 2190: 53–69.

62. Hren MT, Tice MM, Chamberlain CP (2009) Oxygen and hydrogen isotope evidence for a temperature 3.42 billion years ago. *Nature* 462: 205–208.

63. Zhou ZJ, Cameron S, Kadatz B, et al. (1997) Clay swelling diagrams: their applications in formation damage control. *SPE J* 2: 99–106.

64. Sposito G (1984) *The Surface Chemistry of Soils*. New York: Oxford University Press, 115–2208.

65. Joshi PC, Aldersley MF, Delano JW, et al. (2009). Mechanism of montmorillonite catalysis in the formation of RNA oligomers. *J Am Chem Soc* 131: 13369–13374.

66. Hanczyc MM, Fujikawa SM, Szostak JW (2003) Experimental models of primitive cellular compartments: Encapsulation, growth, and division. *Science* 302: 618–622.

67. Hanczyc MM, Mansy SS, Szostak JW (2007) Mineral surface directed membrane assembly. *Orig Life Evol Biosph* 37: 67–82.

68. Mansy SS, Szostak JW (2008) Thermostability of model protocell membranes. *Proc Natl Acad Sci USA* 105: 3351–13355.

69. Guerrini L, Alvarez-Puebla RA, Pazos-Perez N (2018) Surface modifications of nanoparticles for stability in biological fluids. *Materials* 1154.

70. Lombardo D (2009) Liquid-like ordering of negatively charged poly (amidoamine) (PAMAM) dendrimers in solution. *Langmuir* 25: 3271–3275.

71. Lombardo D (2014) Modeling dendrimers charge interaction in solution: Relevance in biosystems. *Biochem Res Int* 2014: 837651.

72. Lombardo D, Calandra P, Magazù S, et al. (2018) Soft nanoparticles charge expression within lipid membranes: The case of amino terminated dendrimers in bilayers vesicles. *Colloids Surf, B* 170: 609–616.

73. Hrenovic J, Milenkovic J, Ivankovic T, et al. (2012) Antibacterial activity of heavy metal-loaded natural zeolite. *J Hazard Mater* 201: 260–264.

74. Hu CH, Xu ZR, Xia MS (2005) Antibacterial effect of Cu^{2+}-exchanged montmorillonite on Aeromonas hydrophila and discussion on its mechanism. *Vet Microbiol* 109: 83–88.

75. Magana SM, Quintana P, Aguilar DH, et al. (2008) Antibacterial activity of montmorillonites modified with silver. *J Mol Catal A Chem* 281: 192–199.

76. Malachová K, Praus P, Rybková Z, et al. (2011) Antibacterial and antifungal activities of silver, copper and zinc montmorillonites. *Appl Clay Sci* 53: 642–645.

77. Morrison KD, Underwood JC, Metge DW, et al. (2014) Mineralogical variables that control the antibacterial effectiveness of a natural clay deposit. *Environ Geochem Health* 36: 613–631.

78. Tong G, Yulong M, Peng G, et al. (2005) Antibacterial effects of the Cu (II)-exchanged montmorillonite on Escherichia coli K88 and Salmonella choleraesuis. *Vet Microbiol* 105: 113–122.

79. Williams LB, Haydel SE (2010) Evaluation of the medicinal use of clay minerals as antibacterial agents. *Int Geol Rev* 52: 745–770.

80. Liyanapatirana C, Gwaltney SR, Xia K (2009) Transformation of triclosan by Fe (III)-saturated montmorillonite. *Environ Sci Technol* 44: 668–674.

81. Qin C, Troya D, Shang C, et al. (2014) Surface catalyzed oxidative oligomerization of 17 β -estradiol by Fe^{3+}-saturated montmorillonite. *Environ Sci Technol* 49: 956–964.

82. Qin C, Chen C, Shang C, et al. (2018) Fe^{3+}-saturated montmorillonite effectively deactivates bacteria in wastewater. *Sci Total Environ* 622–623: 88–95.

83. Majorek KA, Porebski PJ, Dayal A, et al. (2012) Structural and immunologic characterization of bovine, horse, and rabbit serum albumins. *Mol Imm* 52: 174–182.

84. Benkő M, Varga N, Sebők D, et al. (2015) Bovine serum albumin-sodium alkyl sulfates bioconjugates as drug delivery systems. *Coll Surf B Biointerf* 130: 126–132.

85. Xu W, Peng J, Ni D, et al. (2020) Preparation, characterization and application of levan/montmorillonite biocomposite and levan/BSA nanoparticle. *Carb Polym* 234: 115921.

86. Minutoli L, Altavilla D, Bitto A, et al. (2008) Trehalose: A biophysics approach to modulate the inflammatory response during endotoxic shock. *Eur J Pharm* 589: 272–280.

87. Maisano G, Majolino D, Migliardo P, et al. (1993) Sound velocity and hydration phenomena in aqueous polymeric solutions. *Mol Phys* 78: 421–435.

88. Magazù S, Migliardo F, Affouard F, et al. (2010) Study of the relaxational and vibrational dynamics of bioprotectant glass-forming mixtures by neutron scattering and molecular dynamics simulation. *J Chem Phys* 132: 184512.

89. Adamo A, Calabrò E, Magazù S (2019) Thermostabilization of BSA in TMAO water mixtures by infrared spectroscopy. *Curr Chem Biol* 13: 49–59.

90. Magazù S, Caccamo MT (2019) Study of trehalose effects on bsa solutions. In Łopieńska-Biernat E., Stryiński R., *Trehalose: Sources, Chemistry and Applications*, Hauppauge: Nova Science Publishers, 43–62.

91. Magazù S, Migliardo F, Benedetto A, et al. (2013) Protein dynamics by neutron scattering: The protein dynamical transition and the fragile-to-strong dynamical crossover in hydrated lysozyme. *Chem Phys* 424: 26–31.

92. Magazù S, Migliardo F, Benedetto A (2011) Puzzle of protein dynamical transition. *J Phys Chem B* 115: 7736–7743.

93. Fenimore PW, Frauenfelder H, Magazù S, et al. (2013) Concepts and problems in protein dynamics. *Chem Phys* 424: 2–6.

94. Magazù S, Calabro E, T Caccamo M, et al. (2016) The shielding action of disaccharides for typical proteins in aqueous solution against static, 50 Hz and 1800 MHz frequencies electromagnetic fields. *Curr Chem Biol* 10 : 57–64.

95. Magazù S, Migliardo F, Benedetto A, et al. (2013) Bioprotective effects of sucrose and trehalose on proteins. In Magazù, S., *Sucrose: Properties, Biosynthesis and Health Implications*, Hauppauge: Nova Science Publishers, 43–62.

96. Cannuli A, Caccamo MT, Magazù S (2018) Modeling and self-organization dynamics of aggregation processes in acoustically levitated disaccharides solutions. *AAPP Atti della Accademia Peloritana dei Pericolanti, Classe di Scienze Fisiche, Matematiche e Naturali*, 96: 3.

97. Squire PG, Maser P, O'Konski CT (1968) The hydrodynamic properties of bovine serum albumin monomer and dimmer. *Biochem* 7: 4261–4272.

98. De Paz RA, Dale DA, Barnett CC, et al. (2002) Effects of drying methods and additives on the structure, function, and storage stability of subtilisin: role of protein conformation and molecular mobility. *Enzyme Microb Technol* 31: 765–774.

99. Xu Y, Hanna MA (2008) Morphological and structural properties of two-phase coaxial jet electrosprayed BSA-PLA capsules. *J Microencapsul* 25: 469–477.

100. Kopac T, Bozgeyik K, Yener J (2008) Effect of pH and temperature on the adsorption of bovine serum albumin onto titanium dioxide. *Coll Surf Physicochem Engin Aspects* 322: 19–28.

101. Yohannes G, Wiedmer SK, Elomaa M, et al. (2010) Thermal aggregation of bovine serum albumin studied by asymmetrical flow field-flow fractionation. *Anal Chim Acta* 675: 191–198.

102. Alkan M, Demirbas O, Dogan M, et al. (2006) Surface properties of bovine serum albumin—adsorbed oxides: Adsorption, adsorption kinetics and electrokinetic properties. *Micro Meso Materials* 96: 331–340.

103. Magazù S, Migliardo F, Benedetto A (2011) Elastic incoherent neutron scattering operating by varying instrumental energy resolution: Principle, simulations, and experiments of the resolution elastic neutron scattering (RENS). *Rev Sci Instr* 82: 105115.

104. Migliardo F, Magazù S, Caccamo MT (2013) Infrared, Raman and INS studies of poly-ethylene oxide oligomers. *J Mol Struc* 1048: 261–266.

105. Calabrò E, Condello S, Currò M, et al. (2013) Effects of low intensity static magnetic field on FTIR spectra and ROS production in SH-SY5Y neuronal-like cells. *Bioelectromagn* 34: 618–629.

106. Varga B, Migliardo F, Takacs E, et al. (2008) Neutron scattering studies on dUTPase complex in the presence of bioprotectant systems. *Chem Phys* 345: 250–258.

107. Cannuli A, Caccamo MT, Castorina G, et al. (2018) Laser techniques on acoustically levitated droplets. *EPJ Web of Confer* 167: 5010.

108. Egli M (2016) Diffraction techniques in structural biology. *Curr Protoc Nucleic Acid Chem* 65: 7.13.1–7.13.41.

109. Dong M, Husale S, Sahin O (2009) Determination of protein structural flexibility by microsecond force spectroscopy. *Nature nanotechn* 4: 514–517.

110. Becker W, Bhattiprolu KC, Gubensäk N, et al. (2018) Investigating protein-ligand interactions by solution nuclear magnetic resonance spectroscopy. *Chemphyschem: Eur J Chem Phys Phys Chem* 19: 895–906.

111. Magazù S, Maisano G, Migliardo F, et al. (2008) Elastic incoherent neutron scattering on systems of biophysical interest: Mean square displacement evaluation from self-distribution function. *J Phys Chem B* 112: 8936–8942.

112. Caccamo MT, Magazù S (2018) Applications of wavelet analyses on spectroscopic experiments. In: Burgess, J., *Wavelets: Principles, Analysis and Applications*, Hauppauge: Nova Science Publishers, 77–90.

113. Caccamo MT, Magazù S (2016) Tagging the oligomer-to-polymer crossover on EG and PEGs by infrared and Raman spectroscopies and by wavelet cross-correlation spectral analysis. *Vib Spectr* 85: 222–227.

114. Caccamo MT, Zammuto V, Gugliandolo C, et al. (2018) Thermal restraint of a bacterial exopolysaccharide of shallow vent origin. *Int J Biol Macromol* 114: 649–655.

115. Magazù S, Calabrò E, Caccamo MT (2018) Experimental study of thermal restraint in bio-protectant disaccharides by FTIR spectroscopy. *Open Biotech J* 12: 123–133.

116. Magazù S, Migliardo F, Vertessy BG, et al. (2013) Investigations of homologous disaccharides by elastic incoherent neutron scattering and wavelet multiresolution analysis. *Chem Phys* 424: 56–61.

117. Migliardo F, Caccamo MT, Magazù S (2014) Thermal analysis on bioprotectant disaccharides by elastic incoherent neutron scattering. *Food Biophys* 9: 99–104.

118. Veleda D, Montagne R, Araujo M (2012) Cross-wavelet bias corrected by normalizing scales. *J Atmos Ocean Technol* 29: 1401–1408.

119. Caccamo MT, Cannuli A, Magazù S (2018) Wavelet analysis of near-resonant series RLC circuit with time-dependent forcing frequency. *Eur J Phys* 39: 045702.

120. Migliardo F, Caccamo MT, Magazù S (2013) Elastic incoherent neutron scatterings wavevector and thermal analysis on glass-forming homologous disaccharides. *J Non-Cryst Solids* 378: 144–151.

121. Torrence C, Compo GP (1998) A practical guide to wavelet analysis. *Bull Am Meteorol Soc* 79: 61–78.

122. Grinsted A, Moore JC, Jevrejeva S (2004) Application of the cross wavelet transform and wavelet coherence to geophysical time series. *Nonlin Processes Geophys* 2004: 561–566.

123. Magazù S, Caccamo MT (2018) Fourier and wavelet analyses of climate data. In Magazù, S., *New Trends in Physics Education Research*; Hauppauge: Nova Science Publishers, 225–242.

124. Caccamo MT, Magazù S (2018) Variable length pendulum analyzed by a comparative Fourier and wavelet approach. *Rev Mex Fis E* 64: 81–86.

125. Colombo F, Magazù S, Caccamo MT (2018)Wavelet analysis as a tool for characterizing trends in climatic data, In: Burgess, J., *Wavelets: Principles, Analysis and Applications,* Hauppauge: Nova Science Publishers, 55–76.